Asian Journal of Current Research in Clinical Cancer
ISSN: 3062-4444
2022, Volume 2, Issue 2, Page No: 89-100

Available online at: www.galaxypub.co/page/journals

Galaxy Publication

Galaxy Publication

Integrating Clinical and Diffusion-Weighted MRI Radiomics via Machine Learning for Predicting Lymph Node Metastasis in Endometrial Cancer

G. Papadopoulos[1*], N. Vlachos[1], E. Georgiou[1]

[1]Department of Clinical Oncology, School of Medicine, University of Athens, Athens, Greece.

***E-mail** ✉ athens.clinonc.21@emailprovider.net

Received: 07 September 2022; **Revised:** 26 November 2022; **Accepted:** 01 December 2022

ABSTRACT

Effective evaluation of lymphadenectomy risk is crucial in managing endometrial cancer (EC), as it requires balancing therapeutic outcomes with the potential for surgical complications and mortality. This study aimed to determine the additional diagnostic benefit of employing computer-assisted image segmentation combined with machine learning techniques that merge clinical indicators and diffusion-weighted magnetic resonance imaging (DWI-MRI) radiomic data for forecasting lymph node (LN) metastasis in EC. A total of 236 women diagnosed with EC (average age 51.2 ± 11.6 years) who underwent preoperative MRI between July 2010 and July 2018 were prospectively enrolled. Participants were randomly allocated into a training group (n = 165) and a validation group (n = 71). A decision tree classifier was established using several features: the tumor's mean apparent diffusion coefficient (ADC; cutoff 1.1 × 10^{-3} mm^2/s), relative ADC skewness (cutoff 1.2), LN short-axis diameter (cutoff 1.7 mm), LN ADC skewness (cutoff 7.2 × 10^{-2}), tumor grade (grade 1 versus grades 2–3), and clinical tumor diameter (cutoff 20 mm). The model demonstrated sensitivities of 94% (training) and 86% (validation) and specificities of 80% and 78%, respectively. Its diagnostic performance, indicated by an area under the ROC curve (AUC) of 0.85, significantly outperformed both the mean ADC-based model (AUC = 0.54) and LN short-axis diameter criteria (AUC = 0.62) ($p < 0.0001$). In summary, integrating clinical factors with MRI-derived radiomic attributes using a machine learning approach provides a superior framework for predicting LN metastasis in EC compared to conventional ADC and size assessments.

Keywords: Computer-assisted analysis, Diffusion-weighted MRI, Endometrial carcinoma, Lymphatic metastasis, Artificial intelligence, Radiomics

How to Cite This Article: Papadopoulos G, Vlachos N, Georgiou E. Integrating Clinical and Diffusion-Weighted MRI Radiomics via Machine Learning for Predicting Lymph Node Metastasis in Endometrial Cancer. Asian J Curr Res Clin Cancer. 2022;2(2):89-100. https://doi.org/10.51847/ZiZPj56i2s

Introduction

Endometrial cancer (EC) represents one of the most prevalent malignancies affecting the female reproductive system globally. Its incidence continues to rise, particularly in nations undergoing rapid economic and social development [1]. While early-detected EC generally carries a favorable prognosis [2], the presence of lymph node (LN) metastasis significantly worsens patient outcomes. Lymphadenectomy remains a crucial step for determining nodal involvement and planning appropriate adjuvant therapy [2]. Nevertheless, the necessity of performing routine lymphadenectomy in all EC cases is still debated [3, 4], mainly because of postoperative complications and the challenges posed by obesity during surgery. On the other hand, recent studies indicate that patients at intermediate or high risk of nodal metastasis may benefit from systematic lymph node removal [5]. These findings emphasize the need for accurate preoperative risk stratification to optimize treatment benefits while minimizing surgical morbidity and mortality.

Magnetic resonance (MR) imaging plays an important role in assessing nodal spread and defining the anatomical boundaries for lymphadenectomy [6]. However, conventional MR methods, which typically identify suspicious nodes using a short-axis diameter threshold of 10 mm or greater, show limited diagnostic sensitivity—around 48% [7]. Diffusion-weighted (DW) imaging has improved the visualization of pelvic lymph nodes [8, 9]; yet, the

clinical utility of apparent diffusion coefficient (ADC) values in predicting LN metastasis in EC remains controversial. Some investigations have demonstrated that metastatic nodes display significantly lower mean [10] and relative [11] ADC values compared to benign nodes, whereas others have reported conflicting outcomes [9]. These inconsistencies may stem from interobserver and intraobserver variability in ADC measurements [12]. Reliable quantification is further hindered by the typically small size of lymph nodes. Enhancing DW imaging performance in LN assessment thus requires methodological refinement.

Whole-tumor volumetric segmentation offers a more reproducible analytical approach than traditional region-of-interest (ROI) selection. By applying computer-assisted segmentation techniques based on objective imaging characteristics, more consistent LN delineation can be achieved. Additionally, extracting high-dimensional radiomic ADC features and applying machine learning algorithms enables the development of predictive models that can assist in lymphadenectomy planning and localize potential metastatic nodes.

The present study aimed to evaluate the added diagnostic benefit of integrating computer-aided segmentation and machine learning using clinical and diffusion-weighted MR imaging radiomic parameters to predict nodal metastasis in patients with endometrial cancer.

Materials and Methods

Patients and imaging protocol

This prospective observational study included patients diagnosed with endometrial cancer between July 2010 and July 2018 at a tertiary referral hospital, managed by a multidisciplinary team specializing in gynecologic oncology. Ethical approval was obtained from the institutional review board (approval numbers: IRB101-2187B and IRB103-7316A3), and all participants provided written informed consent.

Eligibility criteria included: (1) histopathologically confirmed, untreated EC scheduled for surgery, and (2) age of 18 years or older. Patients were excluded if they had (1) contraindications to MR imaging (such as cardiac pacemakers, insulin pumps, cochlear implants, or metallic foreign bodies), (2) metal prostheses in the pelvis or hip, (3) renal impairment with an estimated glomerular filtration rate below 60 mL/min/1.73 m^2, or (4) inability to give informed consent.

A schematic of the patient selection process is illustrated in **Figure 1**. All imaging studies were performed prior to surgery using a 3.0-Tesla MR scanner (Tim Trio; Siemens, Erlangen, Germany).

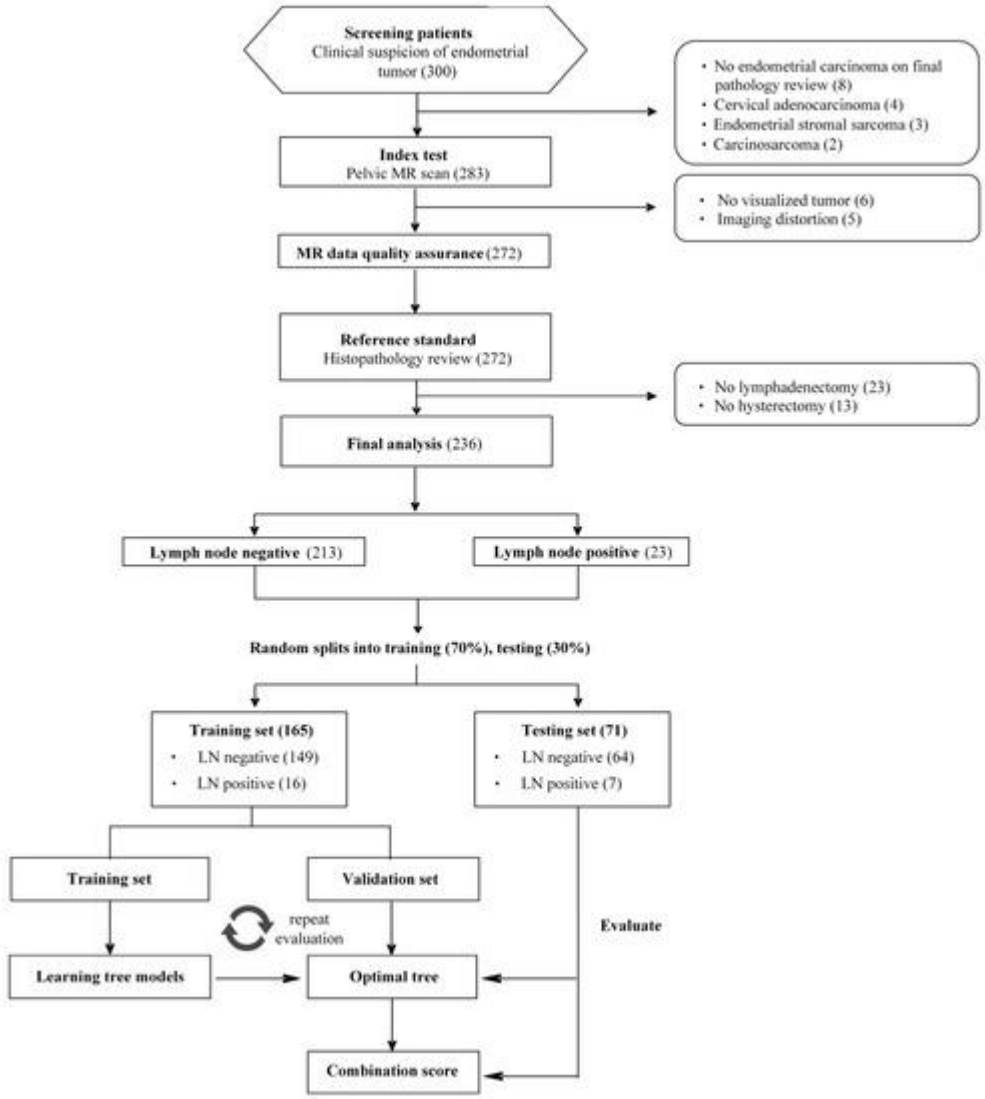

Figure 1. Flowchart of study population. TP = true positive, TN = true negative, FP = false positive, FN = false negative.

Image processing and feature extraction

Image data were analyzed using proprietary software built in MATLAB (version 8.3 R2014a; MathWorks, Natick, MA, USA). The primary tumors were manually outlined on diffusion-weighted sequences to define the regions of interest (ROIs). For lymph nodes (LNs), the largest visible nodes in each region were isolated using an automated segmentation algorithm developed in-house **(Figure 2)**.

To reduce intersubject variation in apparent diffusion coefficient (ADC) measurements, all values were normalized, producing normalized ADC (nADC) metrics. Four principal ADC feature groups were generated: (1) tumor ADC (ADCt), (2) LN ADC (ADCln), (3) the absolute difference in ADC between the tumor and its corresponding LN (rADC), and (4) the absolute difference between the tumor's mean ADC and the histogram-derived ADC values of the LN (rmADC).

Each feature group included twelve histogram-based descriptors—mean, minimum, and maximum ADC; the 10th, 25th, 50th, 75th, and 90th percentile values; skewness; kurtosis; standard deviation; and variance—resulting in 48 features in total. These were further adjusted using the bladder ADC for internal normalization, yielding a total of 96 ADC-associated indices.

Beyond diffusion metrics, six anatomic parameters derived from MRI were evaluated, including tumor volume and five LN morphology measures (area, long-axis length, short-axis length, average diameter, and the short-to-long axis ratio).

Preoperative clinical characteristics were also incorporated, comprising seven routinely available factors: histological type [6, 13, 14]; tumor grade [13–21]; tumor dimension [18, 20, 22]; presence of a lesion in the lower

uterine segment [13, 22]; depth of myometrial invasion [6, 13, 14, 16, 18–22]; radiologic LN status from MRI interpretation [6]; and serum CA-125 concentration [6, 13, 15–17].

Combining all clinical, anatomical, and diffusion-derived parameters produced a comprehensive dataset of **109 input variables** used for subsequent machine learning model development.

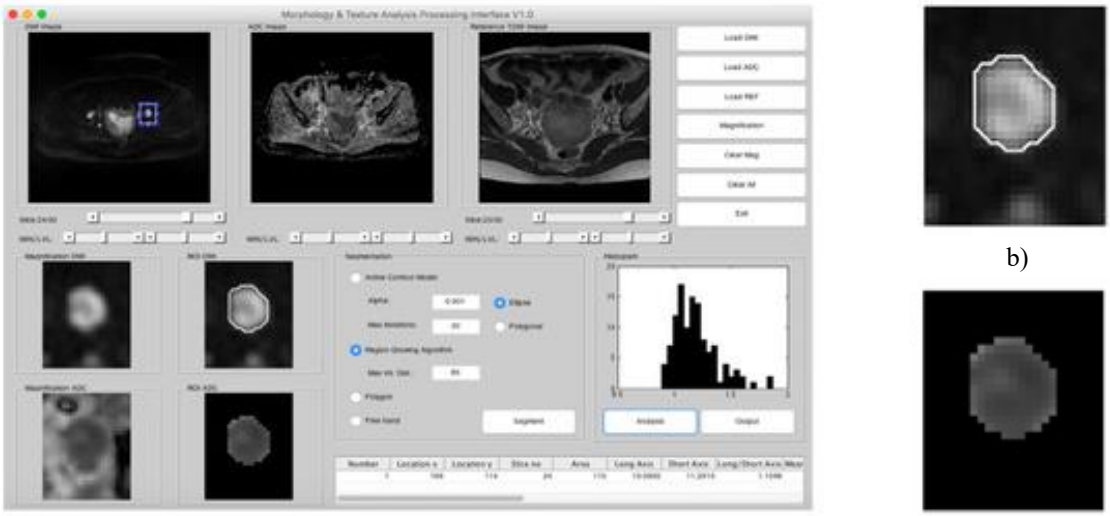

a) b) c)

Figure 2. Automated segmentation of lymph nodes (LNs) was conducted using a computer-assisted approach applied to diffusion-weighted (DW) imaging.

(a) A customized graphical user interface employing a region-growing algorithm enabled LN delineation. Apparent diffusion coefficient (ADC) values obtained from the segmented node were used for histogram-based assessment. The software automatically calculated the LN's short and long axes.

(b) The algorithm accurately identified LN boundaries on the DW image.

(c) An ADC map was generated based on the segmentation results shown in (B).

Histopathology

Final histopathological results served as the reference standard for nodal status confirmation. All patients underwent standardized surgical procedures. Surgeons, having prior access to MR imaging findings, carefully evaluated and excised any lymph nodes suspected of metastasis during pelvic lymphadenectomy.

Statistical analysis

Descriptive statistics were applied to summarize demographic and clinical characteristics. Continuous variables following a normal distribution were analyzed using the *t*-test, while non-parametric data were compared using the Mann–Whitney U test. Categorical variables were examined using the Chi-square or Fisher's exact test, as appropriate.

A weighted decision-tree classifier based on the classification-and-regression-tree (CART) method was employed to construct the predictive model for lymph node (LN) metastasis. The dataset comprising 236 patients was randomly divided into a training group (n = 165; 16 LN-positive, 149 LN-negative) and a testing group (n = 71; 7 LN-positive, 64 LN-negative).

Feature selection and cutoff determination were performed using a region-based decision-tree algorithm that initially incorporated all MR-derived variables to develop a preliminary Radiomic Score (RadScore). The rpart package in R [23] was used to fit the model with parameters set at *cp* = 0.01, *minsplit* = 5, and *maxdepth* = 4. Ten-fold cross-validation, repeated ten times, was conducted to identify the optimal configuration. The binary RadScore provided case classification according to the decision-tree rules and was subsequently combined with clinical parameters to establish an integrated predictive model, termed the Radiomic Signature (RadSignature).

The model was optimized to achieve high sensitivity and negative predictive value (NPV) while maintaining comparable specificity to conventional diagnostic criteria. Model performance was evaluated internally during training and then tested on the independent validation dataset. Diagnostic quality indicators—including sensitivity, specificity, and accuracy—were calculated with 95% confidence intervals (CIs) for both the decision-

tree model and the two single-parameter reference models: the ADC-based model (ADC model) and the short-axis-diameter model (SA model).

Thresholds for ADC and SA were selected using the Youden index. Comparative diagnostic performance was evaluated through receiver-operating-characteristic (ROC) analysis, and the areas under the curve (AUCs) were compared via the De Long test. All analyses were two-tailed, with $p < 0.05$ considered statistically significant. Statistical processing was carried out using SPSS version 11 (SPSS Inc., Chicago, IL, USA), MedCalc version 9.2.0.0 (MedCalc Software, Mariakerke, Belgium), and R version 3.4.1 (R Foundation for Statistical Computing, Vienna, Austria).

Results and Discussion

Demographics

Between July 2010 and July 2018, a total of 300 patients with endometrial cancer were prospectively enrolled. After applying inclusion and exclusion criteria, 236 patients remained eligible for final analysis. The mean ± standard deviation age was 51.2 ± 11.6 years.

A summary of clinical and demographic data is presented in **Table 1**. The mean interval between MR examination and surgical intervention was 27 ± 4 days.

Table 1. Demographics of the study participants.

Variables	RadScore			p-Value
	All	Negative	Positive	
n	236 (100.0)	213 (90.3)	23 (9.7)	
Age (year, mean ± SD)	51.2 ± 11.6	50.6 ± 11.8	56.2 ± 7.7	0.004 *
Histology				<0.0001 *
Non-endometrioid type	17 (7.2)	9 (3.8)	8 (3.4)	
Endometrioid type	219 (92.8)	204 (86.5)	15 (6.3)	
Grade				<0.0001 *
3	44 (18.6)	30 (12.7)	14 (5.9)	
1 + 2	192 (81.4)	183 (77.6)	9 (3.8)	
Tumor size ≥ 20 mm				0.009 *
Presence	140 (59.3)	120 (50.8)	20 (8.5)	
Absence	96 (40.7)	93 (39.5)	3 (1.2)	
Deep myometrial invasion				<0.0001 *
Presence	55 (23.3)	39 (16.6)	16 (6.7)	
Absence	181 (76.7)	174 (73.7)	7 (3.0)	
Low segment involvement				0.002 *
Presence	138 (58.5)	117 (49.6)	21 (8.9)	
Absence	98 (41.5)	96 (40.7)	2 (0.8)	
CA125 (mean ± SD, U/mL)	52.4 ± 202.4	33.2 ± 43.9	230.7 ± 618.2	0.140

SD = standard deviation. * p < 0.05, Data in parenthesis represents percentage.

Data distribution

Across the cohort, an average of 27 lymph nodes per patient was retrieved from the pelvic sidewalls (range: 0–83), totaling 5,078 nodes. Among the 472 distinct nodal regions analyzed, 33 nodes (7.0%) were confirmed positive for metastasis, and 23 patients (9.7%) exhibited pelvic LN involvement according to final pathology. This proportion provided a balanced dataset suitable for machine learning model development.

Patients with nodal metastases differed significantly from those without in several clinical and pathological features **(Table 1)**. Specifically, metastatic cases were older ($p = 0.004$), more frequently displayed non-endometrioid histology ($p < 0.001$), higher tumor grade (grade 3; $p < 0.001$), larger tumor dimensions ($p = 0.009$), deep myometrial invasion ($p < 0.0001$), and involvement of the lower uterine segment ($p = 0.002$). Stepwise

multivariate regression identified non-endometrioid histology and deep myometrial invasion as independent predictors of nodal metastasis.

Morphometric assessment of the lymph nodes revealed that metastatic nodes had significantly greater short-axis diameters ($p < 0.0001$) and higher short-to-long axis ratios ($p < 0.0001$) compared with benign nodes. Tumor diffusion metrics also differed: ADCmean ($p < 0.0001$) and ADCmin ($p = 0.003$) were significantly lower in tumors associated with positive nodes, whereas ADCmax showed no significant distinction ($p = 0.316$). ADC values within metastatic lymph nodes were reduced relative to benign nodes (ADCmean, $p = 0.049$; ADCmin, $p = 0.017$). Correlation analysis demonstrated strong interdependence among ADC features. None of the analyzed nodes displayed morphological signs such as lobulation or spiculation that could independently indicate metastasis.

Model construction and subgroup analysis

Using decision-tree methodology, a Radiomic Score (RadScore) was derived from quantitative imaging parameters. This score incorporated: mean tumor ADC (ADCtmean; threshold 1.1 × 10^{-3} mm²/s), skewness of relative tumor ADC (rADCskewness; threshold 1.2), short-axis diameter of the lymph node (threshold 1.7 mm), and skewness of LN ADC (ADClnskewness; threshold 7.2 × 10^{-2}) **(Figure 3a)**. The distribution of patients according to RadScore-defined risk levels is detailed in **Table 2**.

To enhance predictive performance, a composite Radiomic Signature (RadSignature) was created by combining the RadScore with key clinical factors: tumor grade (grades 1–2 versus grade 3) and tumor size (threshold 20 mm). This integrative model aimed to provide more accurate stratification of patients at risk for lymph node metastasis **(Figure 3b)**.

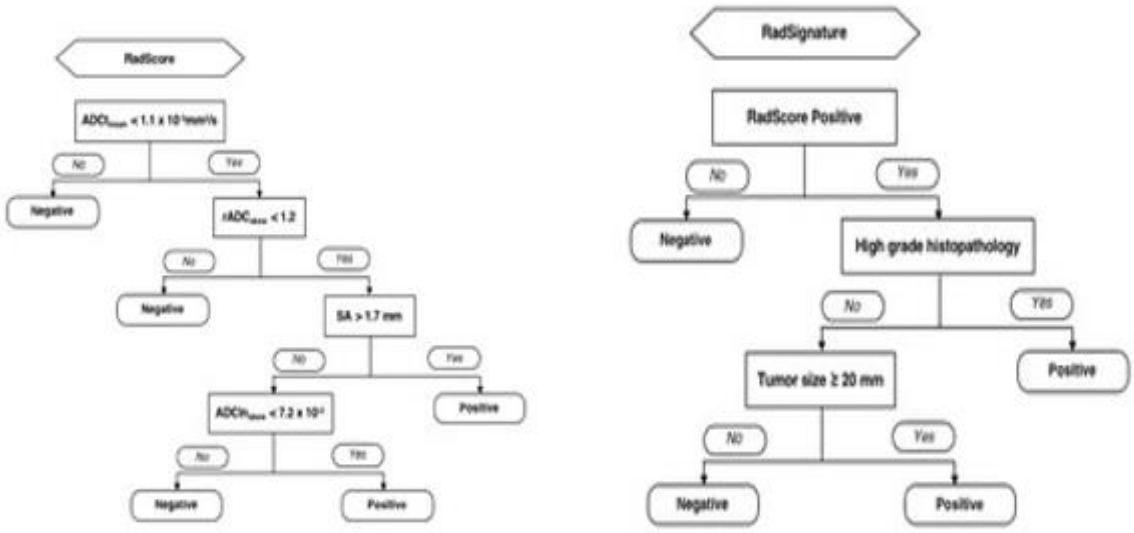

a) b)

Figure 3. The development of RadSignature to predict lymph node metastasis in endometrial cancer patients. The RadScore was developed based on image only radiomics classification and regression tree analysis (a) The RadSignature was determined by combination of RadScore and clinical parameters (b) The rpart package in R was used, and 10-fold cross-validation process repeated 10 times to select the best fitting.

Table 2. Characteristics of patients according to the risk group based on radiomics parameters (RadScore).

Variables	Lymph Node Metastasis			p-Value
	All	Absent	Present	
n	236 (100.0)	151 (64.0)	85 (36.0)	
Age (year, mean ± SD)	51.2 ± 11.6	49.8 ± 11.8	53.6 ± 10.8	0.017 *
Histology				0.005 *
Non-endometrioid type	17 (7.2)	5 (2.1)	12 (5.1)	

Endometrioid type	219 (92.8)	146 (61.9)	73 (30.9)	
Grade				0.049 *
3	44 (18.6)	22 (9.3)	22 (9.3)	
1 + 2	192 (81.4)	129 (54.7)	63 (26.7)	
Tumor size ≥ 20 mm				0.002 *
Presence	140 (59.3)	78 (33.1)	62 (26.2)	
Absence	96 (40.7)	73 (30.9)	23 (9.8)	
Deep myometrial invasion				<0.0001 *
Presence	55 (23.3)	20 (8.5)	35 (14.8)	
Absence	181 (76.7)	131 (55.5)	50 (21.2)	
Low segment involvement				0.015 *
Presence	138 (58.5)	79 (33.5)	59 (25.0)	
Absence	98 (41.5)	72 (30.5)	26 (11.0)	
CA125 (mean ± SD, U/mL)	52.4 ± 202.4	32.4 ± 36.3	87.9 ± 332.0	0.129

SD = standard deviation. * $p < 0.05$, Data in parenthesis represents percentage.

Model performance and diagnostic evaluation

Using bootstrap validation on the training cohort, the RadSignature demonstrated high diagnostic reliability for regional lymph node assessment. It achieved a sensitivity of 95.5% (95% CI: 87.9–100%), specificity of 86.9% (82.8–90.9%), overall accuracy of 87.8% (84.2–91.2%), positive predictive value of 45.1% (38.3–53.4%), and a negative predictive value of 99.4% (98.4–100%).

For context, the ADC-based model used only the mean ADC of the lymph nodes (ADClnmean < 1.1×10^{-3} mm^2/s), while the SA model relied on a short-axis LN diameter threshold exceeding 5 mm.

Analysis of the models' performance in detecting pelvic LN metastasis is summarized in **Table 3**. At the regional level, the RadSignature identified all metastatic nodes (sensitivity 100%), significantly outperforming the ADC model (44%, $p = 0.0001$) and the SA model (76%, $p = 0.0313$). Specificity for RadSignature (91%) was also superior to both the ADC (75%, $p < 0.0001$) and SA models (61%, $p < 0.0001$) in the independent testing set.

When considering individual patients, the RadSignature again achieved complete sensitivity (100%), which was significantly higher than the ADC model (59%, $p = 0.0156$) and numerically higher than the SA model (88%, $p = 0.5$), though the latter did not reach statistical significance. Its patient-level specificity was 90%, exceeding both the ADC (67%, $p = 0.0001$) and SA models (41%, $p < 0.0001$).

Finally, ROC curve analysis confirmed that the RadSignature consistently outperformed both the ADC-only and SA-based models in discriminating metastatic from non-metastatic nodes at both regional and patient levels.

Table 3. Diagnostic accuracy for detecting pelvic lymph node metastasis based on selected magnetic resonance (MR) imaging features.

Variables	**Lymph Node Metastasis**			**p-Value**
	All	**Absent**	**Present**	
n	236 (100.0)	151 (64.0)	85 (36.0)	
Age (year, mean ± SD)	51.2 ± 11.6	49.8 ± 11.8	53.6 ± 10.8	0.017 *
Histology				0.005 *
Non-endometrioid type	17 (7.2)	5 (2.1)	12 (5.1)	
Endometrioid type	219 (92.8)	146 (61.9)	73 (30.9)	
Grade				0.049 *
3	44 (18.6)	22 (9.3)	22 (9.3)	
1 + 2	192 (81.4)	129 (54.7)	63 (26.7)	
Tumor size ≥ 20 mm				0.002 *
Presence	140 (59.3)	78 (33.1)	62 (26.2)	
Absence	96 (40.7)	73 (30.9)	23 (9.8)	
Deep myometrial invasion				<0.0001 *

Presence	55 (23.3)	20 (8.5)	35 (14.8)	
Absence	181 (76.7)	131 (55.5)	50 (21.2)	
Low segment involvement				0.015 *
Presence	138 (58.5)	79 (33.5)	59 (25.0)	
Absence	98 (41.5)	72 (30.5)	26 (11.0)	
CA125 (mean ± SD, U/mL)	52.4 ± 202.4	32.4 ± 36.3	87.9 ± 332.0	0.129

SD = standard deviation. * $p < 0.05$, Data in parenthesis represents percentage.

ROC analysis and insights from false-negative cases

Comparisons of ROC curves for the detection of pelvic lymph node metastasis are presented in **Table 4**. Remarkably, the RadSignature misclassified only two lymph nodes, both of which contained extremely small metastatic deposits, measuring 0.8 mm and 3.3 mm, highlighting the challenge of detecting microscopic disease.

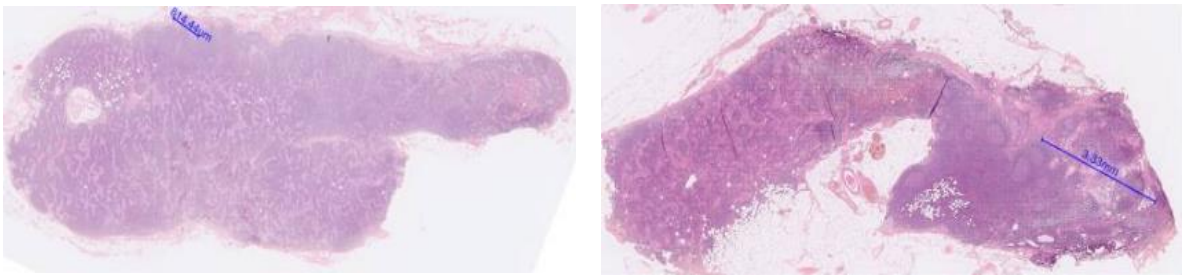

a) b)

Figure 4. Case Examples of RadSignature False Negatives

Case 1: A 40-year-old woman diagnosed with grade 2 endometrioid adenocarcinoma with squamous differentiation, involving both the low uterine segment and cervical stroma, staged T2N1mi. The primary tumor measured 6.5 cm, and serum CA-125 was 37.3 U/mL. According to the RadSignature criteria, this lymph node was classified as negative based on tumor ADCtmean = 0.928×10^{-3} mm²/s, rADCskewness = 0.051, LN short-axis = 1.506 mm, and ADClnskewness = 0.413×10^{-2}. Histopathology revealed a microscopic metastatic focus of 0.8 mm, which was only detectable on hematoxylin and eosin (H&E) staining.

Case 2: A 6-year-old patient with grade 2 endometrioid adenocarcinoma, with neither low segment nor cervical stromal involvement, staged T1bN1a. Tumor size was 1 cm, and CA-125 measured 24.3 U/mL. The lymph node in this case was deemed negative by RadSignature (tumor ADCtmean = 0.779×10^{-3} mm²/s, rADCskewness = 2.3263, LN short-axis = 3.364 mm, ADClnskewness = 2.178×10^{-2}). H&E staining identified a metastatic deposit measuring 3.3 mm.

These examples underscore that while the RadSignature demonstrates high overall sensitivity, it may fail to identify nodes containing very small tumor nests, emphasizing the intrinsic limitation of radiomic detection for sub-millimeter metastases.

Table 4. Pairwise comparisons of ROC curves in detecting pelvic lymph node metastasis.

Variables	AUC Value (95% CI)	p Value
Region basis		
RadSignature	0.89 (0.86–0.92)	
ADC	0.56 (0.52–0.61)	
SA	0.69 (0.64–0.73)	
RadSignature vs. ADC		<0.0001 †
RadSignature vs. SA		<0.0001 †
ADC vs. SA		0.0406
Patient basis		
RadSignature	0.85 (0.80–0.90)	
ADC	0.54 (0.47–0.60)	

SA	0.62 (0.56–0.69)	
RadSignature vs. ADC		<0.0001 †
RadSignature vs. SA		<0.0001 †
ADC vs. SA		0.1742

Data in parentheses are 95% confidence intervals. ROC = receiver operating characteristic, SA = short axis, ADC = mean apparent diffusion coefficient value of the lymph node. † The differences were significant according to Bonferroni correction for multiple comparisons.

Subgroup analysis based on risk categories

Over-diagnosis of lymph node metastasis can lead to unnecessary surgical interventions, especially among patients classified as low-risk. To explore potential over- or under-estimation of nodal involvement, a post-hoc subgroup analysis was performed using criteria from the European Society of Gynaecological Oncology and the European Society for Medical Oncology (ESGO–ESMO) guidelines [24]. Patients were stratified into low-, intermediate-, and high-risk groups according to tumor stage, grade, and histologic type.

Across all subgroups, the RadSignature consistently showed superior performance compared with the ADC-only and short-axis (SA) models. Remarkably, at the patient level, the RadSignature maintained a sensitivity of 100% for detecting lymph node metastasis in each risk category. In the low-risk group, its specificity was significantly greater than that of both the ADC model ($p = 0.0005$) and the SA model ($p < 0.0001$), indicating a reduced likelihood of unnecessary lymph node dissections. Among intermediate- and high-risk patients, the RadSignature also demonstrated higher specificity than the SA model, reaching 86%, with statistical significance ($p = 0.0078$ and $p = 0.0313$, respectively). These findings suggest that the integrated radiomic and clinical model can enhance diagnostic precision and help tailor the extent of lymphadenectomy according to individual risk profiles.

Table 5. Subgroup analysis of diagnostic accuracy of MR imaging for detecting pelvic lymph node metastasis.

Parameters	n	TP	TN	FP	FN	Sensitivity	Specificity	Accuracy
Low risk								
RadSignature	165	4	135	25	1	80.0% (28.4–99.5%)	84.4% (77.8–89.6%)	84.2% (77.8–89.4%)
RadScore	165	4	116	44	1	80.0% (28.4–99.5%)	72.5% (64.9–79.3%)	72.7% (65.3–79.4%)
ADC	165	5	26	134	0	100.0% (47.8–100.0%)	16.3% (10.9–22.9%) *	18.8% (13.1–25.6%) *
SA	165	1	86	74	4	20.0% (0.5–71.6%) *	53.8% (45.7–61.7%) *	52.7% (44.8–60.5%) *
Intermediate risk								
RadSignature	36	3	20	12	1	75.0% (19.4–99.4%)	62.5% (43.7–78.9%)	63.9% (46.2–79.2%)
RadScore	36	3	19	13	1	75.0% (19.4–99.4%)	59.4% (40.6–76.3%)	61.1% (43.5–76.9%)
ADC	36	4	4	28	0	100.0% (39.8–100.0%)	12.5% (3.5–29.0%) *	22.2% (10.1–39.2%) *
SA	36	2	14	18	2	50.0% (6.8–93.2%)	43.8% (26.4–62.3%) *	44.4% (27.9–61.9%) *
High risk								
RadSignature	35	14	14	7	0	100.0% (76.8–100.0%)	66.7% (43.0–85.4%)	80.0% (63.1–91.6%)
RadScore	35	14	14	7	0	100.0% (76.8–100.0%)	66.7% (43.0–85.4%)	80.0% (63.1–91.6%)
ADC	35	12	4	17	2	85.7% (57.2–98.2%)	19.0% (5.4–41.9%) *	45.7% (28.8–63.4%) *
SA	35	14	8	13	0	100.0% (76.8–100.0%)	38.1% (18.1–61.6%) *	62.9% (44.9–78.5%) *

Data in parentheses are 95% confidence intervals. TP = true positive, TN = true negative, FP = false positive, FN = false negative, PPV = positive predictive value, NPV = negative predictive value, SA = short axis, ADC = mean apparent diffusion coefficient value of the lymph node. * $p < 0.05$ McNemar test, as compared with the RadSignature model.

In this study, we developed a composite prediction model, the **RadSignature**, by integrating comprehensive preoperative clinical data with MR imaging parameters. The decision-tree approach was selected for its interpretability, allowing straightforward visualization of binary splits while maintaining a balance between model accuracy and simplicity. Notably, the RadSignature demonstrated a high negative predictive value (98%), suggesting that a subset of low-risk endometrial cancer (EC) patients could potentially avoid lymphadenectomy without compromising diagnostic safety. For those undergoing surgery, the model may assist in planning by indicating the probable laterality of lymph node metastases with reasonable accuracy. To our knowledge, this represents the first preoperative model to predict LN metastasis in EC by combining an extensive set of clinical and radiomic features.

Although the decision tree did not directly incorporate them, we observed that metastatic lymph nodes had significantly lower **ADCmean** and **ADCmin** compared with benign nodes, consistent with prior reports [10]. Other studies have highlighted the utility of ADC metrics, including ADCmin, ADCmax, ADCmean, ADCSD, and relative ADC, in distinguishing metastatic from non-metastatic nodes [25]. However, conflicting evidence exists, with some investigations reporting no significant differences in mean ADC values at either 1.5 T or 3 T [8,9]. These discrepancies may reflect variability in manual measurement, which can be mitigated through the computer-aided segmentation employed in our study.

The **short-axis diameter of lymph nodes** remains a strong predictor of metastasis [10, 26], and it was retained in our decision-tree model. Some prior studies have reported size differences only in pathology specimens rather than on T2-weighted MR images [9], illustrating the potential limitations of conventional imaging. Our use of computer-assisted segmentation addresses this challenge, reducing bias from small region-of-interest selection. Furthermore, combining nodal size with relative ADC values has previously been shown to increase sensitivity for detecting nodal metastasis (25% vs. 83%) without compromising specificity (98% vs. 99%), with the smallest detectable metastatic node measuring 5 mm along its short axis [11].

Consistent with prior literature, **grade I tumors smaller than 20 mm** were highly unlikely to harbor nodal metastases, supporting the use of MR imaging and histologic assessment for identifying low-risk patients who may safely forgo lymphadenectomy [6, 15, 17, 27]. Widely applied criteria, such as the Mayo-modified guidelines—which incorporate differentiation, depth of invasion, and tumor size—further underscore the central role of histologic grade and tumor size in preoperative LN risk assessment [28].

Despite its promise, our model has several limitations. First, the relatively small sample size compared with the number of extracted features may pose a risk of overfitting, though cross-validation and testing on an independent cohort mitigate this concern. Second, the radiomic analysis was limited to histogram-derived ADC features; higher-order texture analyses were not feasible due to the small pixel counts in most lymph nodes (<100 pixels). Third, certain imaging characteristics, such as LN margins, were not incorporated, despite lobulated or spiculated margins being indicative of metastasis. Incorporating these features could further improve model performance. Finally, our study performed region-based analyses without precise node-to-node radiologic-pathologic correlation. Nevertheless, the computer-assisted segmentation approach effectively reduces measurement bias, and the decision-tree framework provides a transparent, interpretable model that balances accuracy and simplicity.

Conclusion

In summary, combining computer-assisted segmentation with machine learning and diffusion-weighted MR radiomics enhances the prediction of lymph node metastasis in endometrial cancer, outperforming conventional ADC and size-based criteria. High-throughput radiomic ADC features, integrated with clinical data, offer a promising tool for preoperative risk stratification and may guide the surgical approach by identifying regions at high risk for nodal involvement.

Acknowledgments: The authors acknowledge the assistance provided by the Cancer Center and Clinical Trial Center, Chang Gung Memorial Hospital, Linkou, Taiwan, which was founded by the Ministry of Health and Welfare of Taiwan MOHW 109-TDU-B-212-114005.

Conflict of Interest: None

Financial Support: This study was funded by Ministry of Science and Technology, Taiwan (grant no.: MOST 104-2314-B-182A-095-MY3 and MOST 109-2628-B-182A-007) and Chang Gung Medical Foundation grant CLRPG3K0021, CLRPG3K0022, CPRPG3G0022, Chang Gung IRB101-2187B and IRB103-7316A3.

Ethics Statement: None

References

1. Lortet-Tieulent J, Ferlay J, Bray F, Jemal A. International patterns and trends in endometrial cancer incidence, 1978–2013. J Natl Cancer Inst. 2018;110(4):354-61.
2. Creasman WT, Odicino F, Maisonneuve P, Quinn MA, Beller U, Benedet JL, et al. Carcinoma of the corpus uteri. FIGO 26th Annual Report. Int J Gynaecol Obstet. 2006;95(Suppl 1):S105-43.
3. Kitchener H, Swart AM, Qian Q, Amos C, Parmar MK. Efficacy of systematic pelvic lymphadenectomy in endometrial cancer (MRC ASTEC trial): Randomised study. Lancet. 2009;373(9658):125-36.
4. Benedetti Panici P, Basile S, Maneschi F, Lissoni A, Signorelli M, Scambia G, et al. Systematic pelvic lymphadenectomy vs no lymphadenectomy in early-stage endometrial carcinoma. J Natl Cancer Inst. 2008;100(23):1707-16.
5. Eggemann H, Ignatov T, Kaiser K, Burger E, Costa SD, Ignatov A. Survival advantage of lymphadenectomy in endometrial cancer. J Cancer Res Clin Oncol. 2016;142(5):1051-60.
6. Kang S, Nam JH, Bae DS, Kim JW, Kim MH, Chen X, et al. Preoperative assessment of lymph node metastasis in endometrial cancer. Cancer. 2017;123(2):263-72.
7. Reijnen C, IntHout J, Massuger L, Strobbe F, Kusters-Vandevelde HVN, Haldorsen IS, et al. Diagnostic accuracy of clinical biomarkers for preoperative prediction of lymph node metastasis in endometrial carcinoma. Oncologist. 2019;24(6):e880-90.
8. Roy C, Bierry G, Matau A, Bazille G, Pasquali R. Value of diffusion-weighted imaging to detect small malignant pelvic lymph nodes at 3T. Eur Radiol. 2010;20(8):1803-11.
9. Nakai G, Matsuki M, Inada Y, Tatsugami F, Tanikake M, Narabayashi I, et al. Detection of pelvic lymph nodes in gynecologic malignancies using diffusion-weighted MRI. J Comput Assist Tomogr. 2008;32(5):764-8.
10. Rechichi G, Galimberti S, Oriani M, Perego P, Valsecchi MG, Sironi S. ADC maps in prediction of pelvic lymph nodal metastasis in endometrial cancer. Eur Radiol. 2013;23(1):65-74.
11. Lin G, Ho KC, Wang JJ, Ng KK, Wai YY, Chen YT, et al. Detection of lymph node metastasis in cervical and uterine cancers by diffusion-weighted MRI at 3T. J Magn Reson Imaging. 2008;28(1):128-35.
12. Kwee TC, Takahara T, Luijten PR, Nievelstein RA. ADC measurements of lymph nodes: Reproducibility study and literature review. Eur J Radiol. 2010;75(2):215-20.
13. Taskin S, Sukur YE, Varli B, Koyuncu K, Seval MM, Ates C, et al. Nomogram to predict lymph node metastasis in endometrial cancer diagnosed incidentally. Arch Gynecol Obstet. 2017;296(4):803-9.
14. Bendifallah S, Canlorbe G, Raimond E, Hudry D, Coutant C, Graesslin O, et al. Impact of LVSI on ESMO risk classification in early endometrial cancer. Br J Cancer. 2014;110(10):2640-6.
15. Son JH, Kong TW, Kim SH, Paek J, Chang SJ, Lee EJ, et al. Prediction of lymph node metastasis in apparent early endometrial cancer. Obstet Gynecol Sci. 2015;58(5):385-90.
16. Tsikouras P, Koukouli Z, Bothou A, Manav B, Iatrakis G, Zervoudis S, et al. Preoperative assessment in endometrial cancer: Is triage for lymphadenectomy possible? J BUON. 2017;22(1):34-43.
17. Lee J, Kong TW, Paek J, Chang SJ, Ryu HS. Predicting lymph node metastasis using preoperative tumor grade, TVUS, and CA-125. Int J Gynecol Cancer. 2016;26(9):1630-5.
18. Zhu M, Jia N, Huang F, Liu X, Zhao Y, Tao X, et al. Are intermediate-risk stage IA EC patients with lesions >2 cm candidates for lymphadenectomy? BMC Cancer. 2017;17(1):696.
19. Oz M, Korkmaz V, Meydanli MM, Sari ME, Cuylan ZF, Gungor T. Impact of tumor size on lymphatic dissemination in grade 1 EC. Int J Gynecol Cancer. 2017;27(7):1393-8.
20. Vargas R, Rauh-Hain JA, Clemmer J, Clark RM, Goodman A, Growdon WB, et al. Prognostic factors of lymph node involvement in endometrial cancer: SEER analysis. Gynecol Oncol. 2014;133(2):216-20.
21. Keys HM, Roberts JA, Brunetto VL, Zaino RJ, Spirtos NM, Bloss JD, et al. Surgery ± external pelvic RT in intermediate-risk endometrial cancer: GOG trial. Gynecol Oncol. 2004;92(3):744-51.

22. Pavlakis K, Rodolakis A, Vagios S, Voulgaris Z, Messini I, Yiannou P, et al. Risk factors for LN metastases in grade 1 endometrial carcinoma. Int J Gynecol Cancer. 2017;27(8):1694-00.
23. Therneau T, Atkinson B, Ripley B. Rpart: Recursive Partitioning and Regression Trees. R package version 4.1-11;2017.
24. Colombo N, Preti E, Landoni F, Carinelli S, Colombo A, Marini C, et al. ESMO guidelines for EC diagnosis, treatment and follow-up. Ann Oncol. 2013;24(Suppl 6):vi33-vi38.
25. Arian A, Easa AM, Arab-Ahmadi M. Diagnostic value of DWI MRI for pelvic LN detection in EC. Acta Radiol. 2020;61(12):1580-6.
26. Rockall AG, Meroni R, Sohaib SA, Reynolds K, Alexander-Sefre F, Shepherd JH, et al. Evaluation of endometrial carcinoma on MRI. Int J Gynecol Cancer. 2007;17(1):188-96.
27. Cignini P, Vitale SG, Lagana AS, Biondi A, La Rosa VL, Cutillo G. Preoperative work-up for lymph node risk in early-stage EC: 5-year follow-up. Updates Surg. 2017;69(1):75-82.
28. Korkmaz V, Meydanli MM, Yalcin I, Sari ME, Sahin H, Kocaman E, et al. Comparison of risk-stratification models for predicting LN involvement in endometrioid EC. J Gynecol Oncol. 2017;28(6):e78.